2950 Niles Road, St. Joseph, MI 49085-9659, USA
269.429.0300 fax 269.429.3852 hq@asabe.org www.asabe.org

An ASABE Meeting Presentation

Paper Number: 096583

Stereo Spectral Imaging System for Plant Health Characterization

Seung-Chul Yoon

USDA, ARS, Richard B. Russell Research Center, Athens, GA 30604-5677, seungchul.yoon@ars.usda.gov

Chi Thai

Dept. of Biological and Agricultural Engineering, University of Georgia, thai@engr.uga.edu

Written for presentation at the
2009 ASABE Annual International Meeting
Sponsored by ASABE
Grand Sierra Resort and Casino
Reno, Nevada
June 21 – June 24, 2009

Abstract. *Three-dimensional (3D) measurements of whole plants may provide detailed structure information about plant health and also complement existing X-ray systems for the below-ground part. In addition to this structure characterization of plants, spectral information may also biochemically characterize plants' health. A stereo vision technique is a cost-effective and rapid imaging technique for measuring and reconstructing 3D structures. The Normalized Difference Vegetation Index (NDVI) requiring measurements of two spectral wavelengths at NIR and red spectral regions has been widely used in remote sensing as an index to estimate various vegetation properties including chlorophyll concentration in leaves, leaf area index, biomass, and plant productivity. We integrated both stereo vision and NDVI techniques and developed a stereo spectral imaging (SSI) system for chlorophyll and biomass quantification of plants in 3D space. We used a stereo vision camera system and custom designed a dual-wavelength filter system at 690 nm and 750 nm to develop the SSI system. Calibration techniques for NDVI computation using two spectral band images were developed by referencing a diffuse reflectance panel. We also developed a texture mapping technique for rendering NDVI values in 3D space. In this paper, the performance of the SSI system was evaluated with an artificial plant showing spectral properties similar to green leaves of real plants.*

Keywords. Stereo, Spectral, NDVI, Stereo Spectral Imaging, Plant, 3D Machine Vision

Introduction

Imaging systems exploiting both stereo vision and spectroscopy have been developed for various agricultural and remote sensing applications and space missions, e.g. autonomous vehicle navigation (Kise and Zhang, 2008), digital elevation maps for land use/cover databases (Paul et al., 2004) and the Surface Stereo Imager for the Phoenix Mars Lander of NASA (Lemmon et al., 2008). In this paper, a stereo spectral imaging (SSI) system collecting and processing spatial and spectral information from two camera views and two spectral bands was developed to study plant health.

3D measurements of whole plant canopies using stereo vision may provide detailed spatial structure information about plant health, disease propagation path, or phenotypes of plants used for biomass production such as cotton, poplar and switch grass, and also complement existing X-ray systems for the below-ground part. In addition to the characterization of plants with 3D spatial information, spectral information may also biochemically characterize plants' health and growth. For example, the normalized difference vegetation index (NDVI) using two spectral reflectance responses at red and near-infrared (NIR) spectral regions has been widely used in remote sensing as an index to estimate various vegetation properties including chlorophyll concentration in leaves (Jones et al., 2007), leaf area index (Drissi et al., 2009), biomass and plant vigor (Boone et al., 2000), plant productivity (Wang et al., 2004), and stress (Plant et al., 2000). We integrated both stereo vision and NDVI techniques and developed a dual-band stereo spectral imaging system for chlorophyll and biomass quantification of plants in 3D space.

Thus, the main objective of the paper was to develop a SSI system that could monitor whole plant canopies in 3D. The specific goals were to reconstruct plant surfaces in 3D space via stereo vision, to acquire spectral features via NDVI, and to map the spectral features onto the 3D data via computer-graphics rendering.

Methods and Materials

Overview of Stereo Spectral Imaging (SSI) System

What is Stereo Vision?

Stereo vision is a cost-effective and rapid imaging technique for measuring and reconstructing object structures in 3D. The fundamental idea of stereo vision is based on the intersection of rays from two views in 3D, assuming that camera intrinsic parameters and the baseline of cameras (relative positions of the cameras) are known (or can be estimated). If an object feature in 3D is visible to both camera views, the feature may appear at different locations on the images captured by the cameras. The amount of spatial displacement, called disparity, is an important cue to obtain the depth of the object feature. Then, depth information is computed directly from disparity values (Trucco and Verri, 1998).

In practice, disparity estimation is performed by a search algorithm, called stereo matching finding correspondence between two separate images. Stereo matching methods to solve this correspondence problem can be categorized into two groups: region correlation-based and feature-based stereo matching. The region correlation-based stereo matching algorithm finds correspondence for every pixel in the image by using pre-determined search windows to compute correlation whereas the feature-based method finds correspondence only for a sparse set of image features (e.g. edges, lines and corners). Two common criteria for correlation computation are the sum of absolute difference (SAD) and the sum of squared difference

(SSD). The SSI system was based on the region correlation-based stereo matching algorithm and the SAD.

What is the normalized difference vegetation index (NDVI)?

Live green plant canopies absorb solar radiation at the blue and red spectral regions for photosynthesis whereas most of the radiation at the spectral region longer than 700 nm is scattered. Hence, images of green plants appear bright in the near-infrared spectral region and dark in the red spectral region. The NDVI was developed to utilize the properties of the different light energy absorption characteristics of plants at the neat-infrared and red spectral regions. The NDVI at each image pixel is obtained by

$$NDVI(x,y) = \frac{\tilde{I}_{\mathrm{NIR}}(x,y) - \tilde{I}_{\mathrm{RED}}(x,y)}{\tilde{I}_{\mathrm{NIR}}(x,y) + \tilde{I}_{\mathrm{RED}}(x,y)}, \tag{1}$$

where $\tilde{I}_{\mathrm{RED}}(x,y)$ and $\tilde{I}_{\mathrm{NIR}}(x,y)$ refer to the calibrated (or normalized) relative reflectance values at the visible (red) and near-infrared spectral regions. The NDVI value itself varies between -1.0 and +1.0. In practice, a value less than 0.2 usually means unhealthy or sparse vegetation and a value close to +1 (more than 0.6) means very healthy green leaves or very dense vegetation. NDVI values for vegetation typically range between 0.2 and 0.7. A zero or less than zero means no vegetation. However, actual wavelengths and bandwidths for NDVI calculations varied with different sensors and applications.

Hardware

The SSI system consisted of a stereo vision camera (Bumblebee XB3, Point Grey Research Inc., Richmond, BC, Canada), a dual-wavelength filter system at 690 nm (red) and 750 nm (NIR) for NDVI computation, a PC and software. The Bumblebee XB3 is a 3 monochrome CCD stereo camera with the IEEE-1394b communication link (800 Mbits/s). Three lenses were horizontally placed 12 cm apart. Thus, three different combinations of baselines were selectable by the user via software: one wide-baseline (24 cm) and two narrow-baselines (12 cm). The lenses were sealed inside the camera unit. The focal length of each lens was set to 3.8 mm. The horizontal field of view of each lens was 70°. The camera was pre-calibrated for lens distortions and camera misalignments. Therefore, there was no need for in-field camera calibration and images were aligned within 0.05 pixel RMS error. The maximum image resolution per lens was 1280x960. Smaller resolutions were selectable by the user via software in order to speed up the stereo processing and to increase the robustness of the stereo processing. The frame transfer rate was 15 frames per second at the full-resolution.

Optical bandpass filters (50.8 mm x 50.8 mm) were used for the NDVI computation. The center wavelengths of the near-infrared and red bandpass filters were 750 nm and 690 nm (20BPF10-690, 20BPF10-750, Newport Corporation, Irvine, CA), respectively. The bandwidths (full width at half maximum) were 13 nm (NIR) and 11 nm (red). Two filter holders were designed and attached to the outside of the camera body such that the filters were placed in front of the lenses to configure the wide-baseline (24 cm apart) setup (fig. 1). The selection of the NIR filter at 750 nm was to avoid the strong signal attenuation due to the oxygen absorption of natural sunlight energy at 760 nm in the consideration of the possibility of deploying the SSI system outdoors and the low quantum efficiency of the CCD sensor beyond 800 nm. Two tungsten halogen lamps (AC) were used as the lighting source in a laboratory setting for this study.

Software

The software was written in C++. The C++ libraries for stereo image acquisition and processing were provided in the Point Grey Research's Software Development Kit (SDK). The graphical user interface of the software was written in the Microsoft Foundation Class 6.0 (or called Visual C++ 6.0). An open source computer vision library, OpenCV 1.0 was used to implement image processing algorithms mentioned in the paper. OpenGL (Shreiner et al., 2005) codes were written for implementing 3D rendering and texture mapping. Figure 1 shows the SSI system setup and a screen capture of the software's graphical user interface.

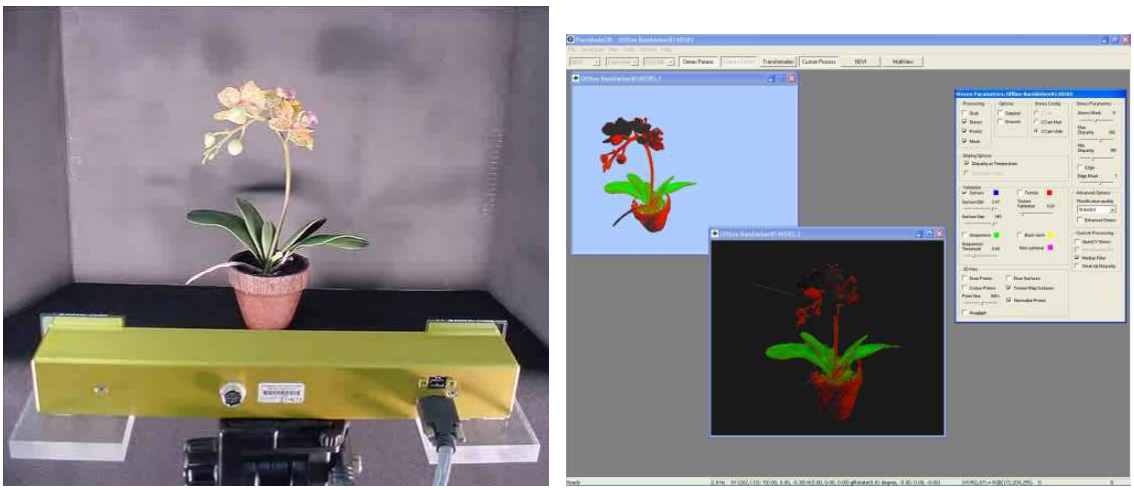

Figure 1. Stereo spectral imaging system setup and software

Stereo Image Acquisition and Processing

Stereo Image Acquisition and Image Calibration

The stereo image processing started from the acquisition of stereo images from two camera views. The NIR-band, red-band, and then raw (un-filtered) stereo images were acquired sequentially at a time by changing the filters manually. In other words, two filters with the same pass-band wavelength were put into the filter holders for acquiring a filtered stereo image. The camera parameters and lighting conditions were not changed during the data acquisition period (except for a flat field calibration to be mentioned later). The captured three stereo images (NIR, red and raw) were used for the following tasks. First, a raw stereo image was used for stereo matching leading to 3D reconstruction. Second, both NIR- and red-filtered stereo images were used for NDVI computation. Third, the NIR-filtered stereo image was used for foreground object segmentation because background clutters were better suppressed by the NIR filter.

The NDVI computation required the intensity calibration (or called normalization) to obtain the relative reflectance at each pixel. We implemented a relative reflectance (RR) calibration method for the SSI system. This method was to calibrate every single pixel on the image by using an 99% diffuse reflectance panel which completely covered the plant object in the field of view. The relative reflectance calibration equation at each pixel required to collect a reference image and a dark current image, and was calculated by

$$\tilde{I}_{measurement}(x,y) = \frac{I_{measurement}(x,y) - I_{dark\ current}(x,y)}{I_{99\%\ reflectance}(x,y) - I_{dark\ current}(x,y)} . \qquad (2)$$

The RR calibration method may be impractical for outdoor applications because it is not possible to put a reflectance panel large enough to cover the area in the entire field of view. Thus, we developed a flat field (FF) calibration technique more suitable for outdoor imaging of plants. The original FF calibration technique (Roberts et al. , 1986) was based on an assumption that the relative reflectance of a calibration target remained unchanged over wavelengths (i.e. red and NIR spectral regions). For the FF calibration, a reflectance target having very little variation in reflectance over wavelengths was placed in the scene and the digital number at each pixel was normalized to the mean value of all pixels in the region of interest (ROI) of the calibration target. The normalization was obtained by

$$\tilde{I}_{NIR}(x,y) = \frac{I_{NIR}(x,y)}{\bar{I}_{A,NIR}},\ \tilde{I}_{RED}(x,y) = \frac{I_{RED}(x,y)}{\bar{I}_{A,RED}}, \tag{3}$$

where $\bar{I}_{A,NIR}$ and $\bar{I}_{A,RED}$ were the average intensity values of the ROI (i.e., the target area A) at the NIR and red spectral bands, respectively. If $\bar{I}_{A,NIR}$ and $\bar{I}_{A,RED}$ are equal (i.e. a constant $\bar{I}_A$) and equation 3 is plugged into equation 1, then the constant $\bar{I}_A$ will be cancelled out and the un-calibrated digital numbers, $I_{\mathrm{RED}}(x,y)$ and $I_{\mathrm{NIR}}(x,y)$ will replace $\tilde{I}_{\mathrm{RED}}(x,y)$ and $\tilde{I}_{\mathrm{NIR}}(x,y)$ in equation 1. For making the average intensity values of the ROI equal (or approximately equal) between two spectral bands, we implemented an algorithm to adjust either a shutter time or a camera gain of the red-band. More specifically, we captured the NIR-band image first and then captured the red-band image by changing a camera parameter (a shutter time or a gain) such that the average intensity value of the ROI in the red-band image becomes (approximately) equal to that in the NIR-band image. The algorithm found an optimal camera parameter for the red-band capture by minimizing the sum of the absolute intensity difference between the ROIs of two bands. Then, the computation of the NDVI became possible with raw digital numbers in the place of normalized values, as defined by

$$\tilde{I}_{NIR}(x,y) = I_{NIR}(x,y),\ \tilde{I}_{RED}(x,y) = \hat{I}_{RED}(x,y), \tag{4}$$

where $\hat{I}_{\mathrm{RED}}(x,y)$ is the intensity value of the red-band image captured after the adjustment of the camera parameter.

Implementation of Stereo Processing

Stereo processing in the SSI system was implemented by using the library functions provided in the Point Grey Research's SDK and OpenCV. The following steps were applied to all 3 stereo images.

First, after two images (8-bit monochrome 1280x960) was captured, they were interleaved into a single image according to a pre-determined image format (2560x960) in order to transfer the data according to the DCAM specification. The acquired stereo images were then pre-processed by a low-pass filter and spatially rectified to un-warp the lens distortions. Without low-pass filtering, the image rectification would produce aliasing effects. After the rectification, the radial image patterns were straightened. This process was applied to all stereo images regardless of using the filters or not.

Second, the rectified NIR-band stereo image was sent to an image segmentation function. For segmentation, an intensity threshold was applied to the rectified stereo image for suppressing out background clutters. Then, a morphological open filter was applied to remove small and

isolated background clutters. The remaining clutters, if remained, were removed manually. Then, this segmentation image was used as a binary mask image applied to all stereo images.

Third, the raw stereo image masked by the segmentation map was sent to the stereo matching algorithm to obtain 3D information of the object in the scene. The stereo matching was based on the sum of absolute difference (SAD) correlation method for estimating disparity at every pixel in the reference view image. The right camera view was used as the reference view image. The secondary (optional) stereo matching was based on the edge detection that utilized the relative difference in intensity values. The output of the stereo matching algorithm was a disparity image. When displaying it, each pixel on the disparity image was mapped by a look-up table representing a close object feature with red and a far-away object feature with blue. The disparity image was represented with either an 8-bit (full-pixel displacement) or 16-bit (sub-pixel displacement) precision.

Fourth, the NIR- and red-band images were input to the NDVI computation engine. Again, they were also masked by the segmentation map. A pseudo-color image was generated by a color look-up table in order to display the resulting NDVI image. The color look-up table of the NDVI values was made according to the following rule.

- If NDVI is less than or equal to 0.2, then grey value. The black refers to -1.
- If NDVI is greater than 0.2 and less than or equal to 0.8, then mixture of pure red (0.2) and pure green (0.8).
- If NDVI is greater than 0.8, then mixture of green and pure blue (1.0).

The float point NDVI values were also saved for future numerical quantification.

Rendering of NDVI Image in 3D

After stereo processing, each pixel in the right camera view (2D) was mapped into a point in the camera coordinate system (3D) where its origin was at the focal point of the right camera. The set of these points in 3D were called point clouds. Obtaining point clouds from stereo matching was the first step for 3D surface reconstruction. Simply, the point clouds were nothing but a set of 3D coordinates representing surface points in 3D. Thus, it was important to spatially connect the surface points in order to create an approximate surface representation. This representation was obtained by a geometric triangular mesh model. Rendering of point clouds and triangular meshes in 3D was implemented by OpenGL functions. The quality of the 3D mesh representation was greatly affected by the quality of generated cloud points. Typically, point clouds needed to be cleaned and edited to remove duplicated and unreferenced points. For this task, when necessary, we removed isolated and tiny surface features by applying a median filer directly to a disparity image. The 3D coordinates of the point clouds were also saved as a standard file format (xyz format) so as to be used in the free open source 3D data processing software (MeshLab) for off-line processing of the point clouds.

Image rendering based on OpenGL was implemented for mapping the computed NDVI values onto 3D point clouds as well as a mesh model in the camera coordinate system such that a 3D virtual image was generated at the any given viewpoint. Also, 3D anaglyph NDVI images were generated in real-time to provide a 3D stereoscopic perception when viewed with two color (red and green) glasses. Figure 2 is the data flowchart of the 3D rendering algorithm of the SSI system.

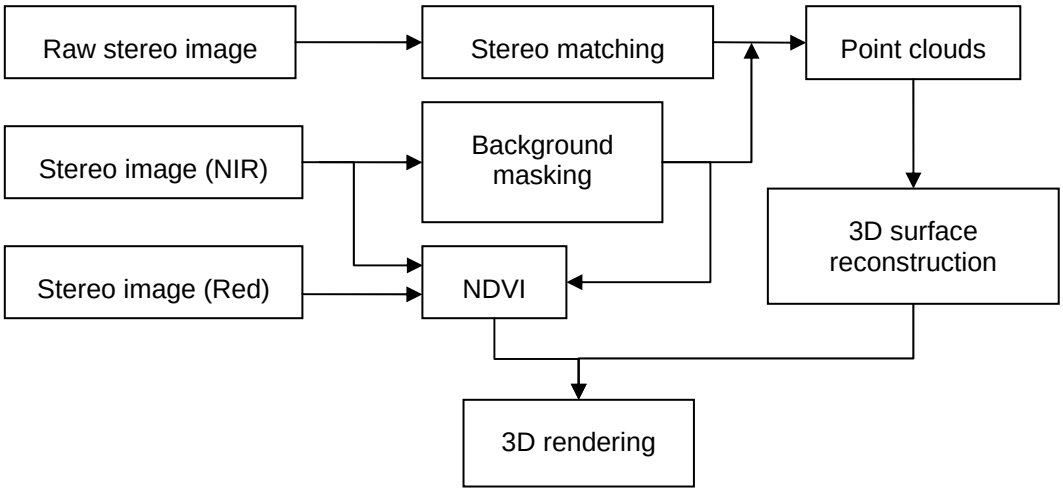

Figure 2. Stereo data flow from acquisition to 3D rendering

Materials

A 99% diffuse reflectance target (SRT-99-180, Spectralon, 18”x18”, Labsphere, North Sutton, NH) was used as the reference material for the relative reflectance (RR) calibration (eq. 2). A 99% diffuse reflectance target (SRT-99-050, Spectralon, 5”x5”, Labsphere, North Sutton, NH) was used as the reference material for the flat field (FF) calibration (eq. 4). For evaluating the RR calibration technique, we used the following seven target materials: a 5”x5” multi-step diffuse reflectance target (SRT-MS-050, Labsphere, North Sutton, NH) having four sub-panels of 99%, 50%, 25% and 12% nominal reflectance values, two vinyl sheets used for military camouflages (uniform dark green and uniform light green) and the back side of the sheets (black). The nominal reflectance values of the vinyl sheets were measured by a four channel fiber-optic spectrometer (SQ2000, Ocean Optics, Dunedin, FL). For evaluating the accuracy of the computed NDVI values, we used the three camouflage vinyl sheets.

An artificial plant (orchid) shown in figure 1 was used for the SSI system development because the leaves of the artificial plant showed spectrally similar reflectance values. Also, it was essential to have a reference plant during the system development cycles because the artificial plant was not perishable and provided good references over time.

Results

Calibration and NDVI Computation

The performance of the RR calibration technique was evaluated by using seven test materials placed in the field of view. The test materials consisted of the multi-step reflectance target (99%, 50%, 25% and 12%) and the two vinyl sheets (dark green, light green) and their back side (black). The performance of the RR calibration was compared with the spectrometer measurements. The calibration of the spectrometer measurements was done on the fly by the Ocean Optics’ software. Calibration values at 689.92 nm and 749.99 nm of the spectrometer were compared against the calibration values of the imaging system at NIR- and red-bands. Figure 3 shows the scatter plot of calibrated image and spectrometer measurements of the test materials. Each point in the figure represented an average calibration value of one particular

material at one of the two spectral wavelengths. Thus, 14 points were obtained. A line obtained by the linear regression model was overlaid to represent the relationship between two instruments. The R^2 value (goodness-of-fit) of the linear regression was 0.9912. Overall, the measured values from the imaging system were slightly lower than the spectrometer measurements. But, the difference was consistently small across the entire calibration value range from 0 to 1.

The calculated NDVI values were evaluated in terms of the RR calibration and the FF calibration by comparing them with NDVI values calculated by the spectrometer. The vinyl sheets (dark green, light green, black) were used as test materials. Figure 4 shows the scatter plot of the NDVI values computed by the SSI system and the spectrometer. Numerical numbers are presented in table 1. A linear regression model was applied to find the linear relationship between two instruments in NDVI computation. The R^2 values of the linear regression were 0.9974 (RR), 0.9921 (FF-Shutter), and 0.9919 (FF-Gain). The performance of the RR calibration was better than the FF calibration methods. However, the FF calibration technique also produced NDVI values close to what the spectrometer produced. In fact, as shown in figure 4, the performance gap among three calibration methods decreased as the NDVI value increased. The overall performance of the SSI system adopting either of three different calibration techniques was similar to that of the spectrometer.

The NDVI values of the sample plant were also measured by the spectrometer. Table 2 summarizes the NDVI values measured at various points of the plant. Five different points were measured for leaf, two different points were measured for stem, and three different points were measured for flower. As shown in table 2, the average and the standard deviation values were obtained. The average NDVI value of the leaf was 0.619 which was similar to normal healthy leaves of green plants. The average NDVI value of the stem was 0.1 less than 0.2. The average NDVI value of the flower (0.041) was even lower than the stem.

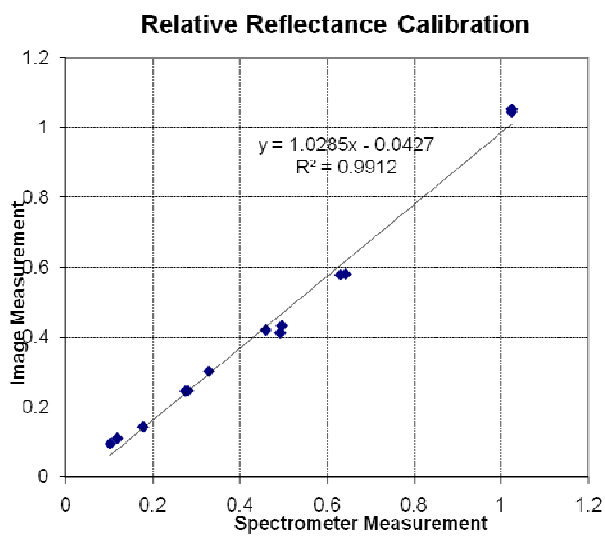

Figure 3. Scatter plot of calibrated relative reflectance measurements of the SSI system and the spectrometer. The coordinates represent normalized relative reflectance. The linear regression line was drawn.

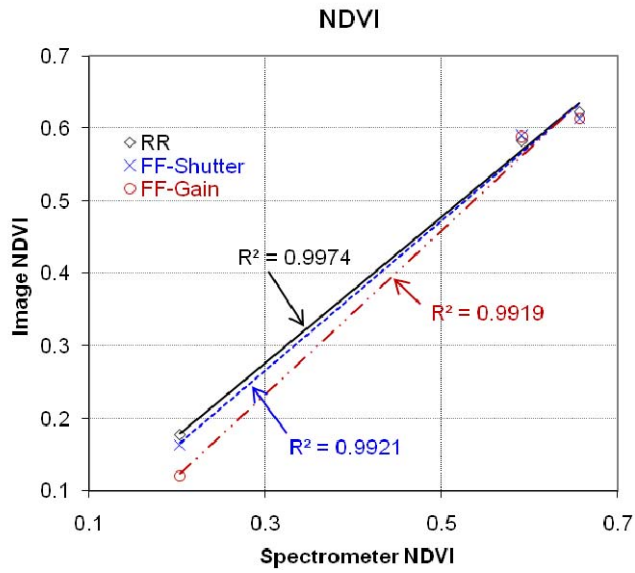

Figure 4. Scatter plot of NDVI values of the SSI system and the spectrometer. The linear regression line was drawn. The "RR" and "FF" refer to the RR and FF calibration-based NDVI calculations, respectively. The "Shutter" and "Gain" refer to one of the FF calibration techniques: shutter time control and gain control.

Table 1. Average NDVI values of the vinyl sheets: SSI system and spectrometer measurements

	Spectrometer-based NDVI	RR-based NDVI	FF-Shutter-based NDVI	FF-Gain-based NDVI
Dark Green	0.656	0.623	0.614	0.612
Light Green	0.591	0.583	0.591	0.588
Back-side	0.203	0.177	0.163	0.121

Table 2. NDVI values of the test sample: spectrometer measurements

	Reflectance at 689.92 nm	Reflectance at 749.99 nm	NDVI
Leaf	0.099 ± 0.063	0.372 ± 0.110	0.619 ± 0.136
Stem	0.135 ± 0.065	0.160 ± 0.048	0.100 ± 0.096
Flower	0.244 ± 0.091	0.261 ± 0.078	0.041 ± 0.059

3D Surface Reconstruction and Rendering

The parameters used for stereo processing of the sample plant were as follows: stereo search window size, 11x11; maximum disparity search range, 302; minimum disparity search limit, 185; image resolution, 512x384; intensity threshold for object segmentation, 8; morphological open filter size, 3. The wide baseline of the stereo camera was used for stereo image acquisition and processing. The synthetic diffuse white light was used for 3D rendering. In OpenGL, the orthographic projection transformation was adopted for 3D rendering. The surface normal vector was computed for providing OpenGL with the correct direction of each mesh's surface. The surface normal vector was positive when the vector direction was coming off the surface (not getting into the surface). The 2D NDVI image (pseudo-color) was input to the OpenGL function for texture mapping of the 3D meshes. The rotation, translation, and zoom in/out by a computer mouse was implemented in the software so that the user can freely move around the 3D object.

Figure 5 shows acquired stereo images: (a) Red-band, (b) NIR-band and (c) raw stereo images. The NIR-band image (fig. 5b) suppressed the background clutters shown in the raw stereo image in figure 5c. The NIR-band image showed a good contrast for segmentation of the plant on the foreground. Figure 6a shows the segmentation result of the plant. This segmentation mask was applied to the subsequent disparity and NDVI images, as shown in figure 6b and 6c, respectively. The disparity map was a pseudo color image similar to temperature. The hotter (red) pixels meant closer to the camera (or viewer). The cooler (blue) pixels meant away from the camera. The NDVI image shown in figure 6c was just a 2D image. As mentioned in table 2, the average NDVI value of the leaves was 0.619 which should be close to green in the NDVI-mapped color image. The blue in figure 6c meant NDVI values greater than 0.8. The stems painted with the red color meant NDVI values close to 0.2. The gray color shown in flower areas meant NDVI values below 0.2. The NDVI values at different parts of the plant were not quantified in this paper but it can be possible by an image segmentation technique for partitioning the plant into multiple segments like leaves, stems and flowers. The 3D rendering results are represented in the point clouds (fig. 6d), the triangle meshes (fig. 6e) and the texture mapping of NDVI values (fig. 6f). The overall quality of the 3D rendering was acceptable with this sample. The imaging system, however, showed difficulties with highly textured plants regardless of real plants or not and still needs to make some improvement.

(a) Red-band stereo image

(b) NIR-band stereo image

(c) Raw stereo image

Figure 5. Stereo images taken with bandpass filters (a and b) and without filters (c). On the left was the right view. On the right was the left view.

The quality of the 3D rendering was greatly dependent on the performance of the stereo matching algorithm. The current stereo vision camera system showed a difficulty in capturing small surface features from highly textured areas due to the inherent limitation of the stereo matching algorithm. Thus, the use of the camera on small plants was challenging. The most important parameter for depth estimation was the min-max range of the disparity values to search for. In order to improve the quality of the 3D rendering, the accuracy of the depth estimation needs to be improved by a better stereo matching algorithm or the point clouds may be cleaned by multiple stereo images taken at different viewpoints.

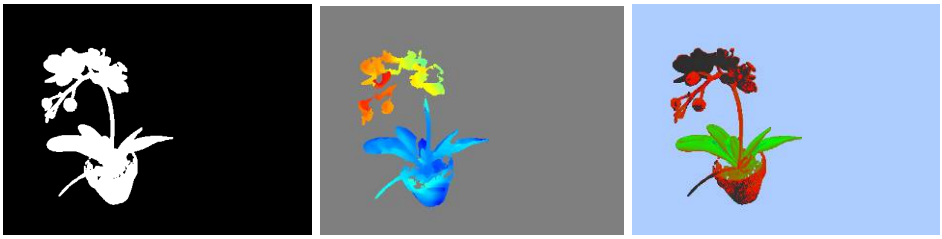

(a) Segmentation mask (b) disparity map (c) NDVI image

(d) Point cloud rendering at different viewpoints

(e) Triangular mesh rendering at different viewpoints

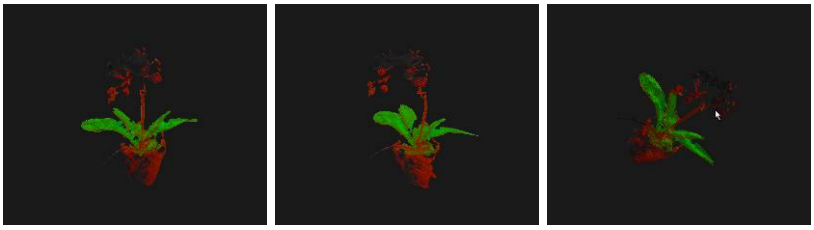

(f) NDVI texture rendering at different viewpoints

Figure 6. Screen captures of the processed images and 3D rendering results. The rendering results at different viewpoints were captured.

Conclusion

We developed a stereo spectral imaging (SSI) system for quantifying plants' health by rendering normalized difference vegetation index (NDVI) values in 3D. We used a stereo vision camera system and custom designed a dual-wavelength filter system at 690 nm and 750 nm to develop the SSI system. The bandpass stereo images of the SSI system were calibrated for the NDVI computation. A new calibration technique based on the flat field calibration was developed for outdoor imaging. The NDVI values measured by the SSI system were compared with the NDVI values measured by a spectrometer. Both performed very similarly (the best goodness-of-fit, R^2 was 0.9974). We also developed a texture mapping technique for rendering NDVI values in 3D. The performance of the SSI system was evaluated with an artificial plant showing spectral properties similar to green leaves of real plants. The test of the SSI system with real plants is planned.

References

Boone, R. B., K. A. Galvin, N. M. Smith, and S. J. Lynn. 2000. Generalizing El Nino effects upon Maasai livestock using hierarchical clusters of vegetation patterns. *Photogrammetric Engineering and Remote Sensing.* 66(6): 737-744.

Drissi, R., J.-P. Goutouly, D. Forget, and J.-P. Gaudillere. 2009. Nondestructive measurement of grapevine leaf area by ground normalized difference vegetation index. *Agronomy Journal*. 101: 226-231.

Jones, C. L., N. O. Maness, M. L. Stone, and R. Jayasekara. Chlorophyll estimation using multispectral reflectance and height sensing. *Transactions of the ASABE*. 50(5): 1867-1872.

Kise, M. and Q. Zhang. 2008. Creating a panoramic field image using multi-spectral stereovision system. *Computers and Electronics in Agriculture*. 60(1): 67-75.

Lemmon, M. T., P. H. Smith, C. Shinohara, R. Tanner, P. Woida, A. Shaw, J. Hughes, R. Reynolds, R. Woida, J. Penegor, C. Oquest, S.F. Hviid, M. B. Madsen, M. Olsen, K. Leer, L. Drube, R. V. Morris, D. Britt. 2008. The Phoenix surface stereo imager (SSI) investigation. In *Proc. 39th Lunar and Planetary Science Conf. (Lunar and Planetary Science XXXIX)*, 1391: 2156-2157.

Paul, F., C. Huggel, and A. Kääb. 2004. Combining satellite multispectral image data and a digital elevation model for mapping debris-covered glaciers. *Remote Sensing of Environment*. 89(4): 510-518.

Plant, R. E., D. S. Munk, B. R. Roberts, R. L. Vargas, D. W. Rains, R. L. Travis, and R. B Hutmacher. 2000. Relationships between remotely sensed reflectance data and cotton growth and yield. *Transactions of the ASAE*. 43(3): 535-546.

Roberts, D. A., Y. Yamaguchi, and R. J. P. Lyon. 1986. Comparison of various techniques for calibration of AIS data. In *Proceedings of the Second Airborne Imaging Spectrometer Data Analysis Workshop*. JPL Publ. 86-35: 21-30.

Shreiner, D., M. Woo, J. Neider, and T. Davis. 2005. *OpenGL(R) Programming Guide: The Official Guide to Learning OpenGL(R), Version 2*. 5th ed. Reading, MA: Addison-Wesley Professional.

Trucco, E. and A. Verri. 1998. *Introductory Techniques for 3-D Computer Vision*. Upper Saddle River, N.J.: Prentice Hall.

Wang, J., P. M. Rich, K. P. Price, and W. D. Kettle. 2004. Relations between NDVI and tree productivity in the central Great Plains. *International Journal of Remote Sen*sing. 25(16): 3127-3138.